HHS Public Access

Author manuscript

*Sci Immunol*. Author manuscript; available in PMC 2019 June 30.

Published in final edited form as:

*Sci Immunol*. 2018 October 05; 3(28): . doi:10.1126/sciimmunol.aat9453.

# The cysteinyl leukotriene 3 receptor regulates expansion of IL-25–producing airway brush cells leading to type 2 inflammation

**Lora G. Bankova**[1,*], **Daniel F. Dwyer**[1], **Eri Yoshimoto**[1], **Saltanat Ualiyeva**[1], **John W. McGinty**[2], **Hannah Raff**[1], **Jakob von Moltke**[2], **Yoshihide Kanaoka**[1], **K. Frank Austen**[1], and **Nora A. Barrett**[1,*]

[1]Division of Rheumatology, Immunology and Allergy, Jeff and Penny Vinik Center for Allergic Disease Research, Brigham and Women's Hospital and Department of Medicine, Harvard Medical School, Boston, MA 02115, USA.

[2]Department of Immunology, University of Washington School of Medicine, Seattle, WA 98109, USA.

## Abstract

Respiratory epithelial cells (EpCs) orchestrate airway mucosal inflammation in response to diverse environmental stimuli, but how distinct EpC programs are regulated remains poorly understood. Here, we report that inhalation of aeroallergens leads to expansion of airway brush cells (BrCs), specialized chemosensory EpCs and the dominant epithelial source of interleukin-25 (IL-25). BrC expansion was attenuated in mice lacking either $LTC_4$ synthase, the biosynthetic enzyme required for cysteinyl leukotriene (CysLT) generation, or the EpC receptor for leukotriene $E_4$ ($LTE_4$), $CysLT_3R$. $LTE_4$ inhalation was sufficient to elicit $CysLT_3R$-dependent BrC expansion in the murine airway through an IL-25–dependent but STAT6-independent signaling pathway. Last, blockade of IL-25 attenuated both aeroallergen and $LTE_4$-elicited $CysLT_3R$-dependent type 2 lung inflammation. These results demonstrate that $CysLT_3R$ senses the endogenously generated lipid ligand $LTE_4$ and regulates airway BrC number and function.

## INTRODUCTION

The exogenous and endogenous cues that trigger immune responsiveness in the respiratory tract are still poorly understood. The cysteinyl leukotrienes (CysLTs) leukotriene $C_4$ ($LTC_4$), $LTD_4$, and $LTE_4$ are lipid mediators recognized for their potent induction of vascular permeability, smooth muscle constriction, and cellular chemotaxis. They are synthesized by effector cells in established allergic airway inflammation (1) through the 5-lipoxygenase (5-



*Corresponding author, lbankova@bwh.harvard.edu (L.G.B.); nbarrett@bwh.harvard.edu (N.A.B.).

**Author contributions:** Conceptualization: L.G.B., K.F.A., and N.A.B.; statistical analysis: L.G.B. and D.F.D.; investigation: L.G.B., E.Y., S.U., N.A.B., J.W.M., H.R., and J.v.M.; writing: L.G.B., D.F.D., N.A.B., J.v.M., K.F.A., and Y.K.; funding acquisition: N.A.B., L.G.B., and Y.K.; resources: Y.K. and J.v.M.

**Competing interests:** The authors declare that they have no competing interests.

**Data and materials availability:** RNA-seq data are available from the Gene Expression Omnibus (GSE116525).

LO)/$LTC_4$ synthase ($LTC_4S$) pathway and elicit bronchoconstriction in asthma through activation of the type 1 cysteinyl leukotriene receptor, $CysLT_1R$ (2–4). However, CysLT generation is also elicited early in the primary immune response to diverse type 2 inflammatory stimuli such as the house dust mite *Dermatophagoides farinae* (*Df*) (5), the mold *Alternaria alternata* (*Alternaria*) (6), the helminth *Nippostrongylus brasiliensis* (7), and chitin (7), a component of the fungal and arthropod cell wall. Furthermore, recent studies have suggested that CysLTs play a role in promoting the development of type 2 inflammation in the airways. $CysLT_1R$ conditions dendritic cells (DCs) for T helper 2 ($T_H2$) priming in response to house dust mite inhalation (5, 8) and augments nuclear factor of activated T cell signaling (NFAT) and type 2 cytokine generation in group 2 innate lymphoid cells (ILC2s) (7, 9, 10), demonstrating activity to promote both innate and adaptive type 2 inflammation. $LTE_4$ triggers ILC2 cytokine production in vivo but is resistant to $CysLT_1R$ blockade (9), indicating involvement of an additional CysLTR. Moreover, $LTE_4$ cannot activate ILC2s in vitro, indicating a distinct site of action (7). Collectively, recent evidence suggests that a nonclassical CysLT receptor expressed on resident cells in the airways promotes type 2 inflammation.

$CysLT_3R$ (also known as OXGR1 or GPR99) is the high-affinity receptor for $LTE_4$ (11). We recently determined that $CysLT_3R$ is expressed on murine airway epithelial cells (EpCs) and mediates goblet cell mucin release in response to exogenous $LTE_4$ or to endogenously generated CysLTs elicited by the fungal aeroallergen, *Alternaria* (6). Furthermore, we identified a distinct role for $CysLT_3R$ in regulating goblet cell numbers in the nasal mucosa that was not shared by the other CysLT receptors. Thus, we hypothesized that $CysLT_3R$ might regulate a proximal EpC-driven inflammatory pathway important in type 2 inflammation.

EpCs orchestrate type 2 immunity at mucosal sites, in part through the production of cytokines interleukin-25 (IL-25), IL-33, and thymic stromal lymphopoietin (TSLP). Tuft cells, a population of chemosensory EpCs, were recently recognized as the dominant epithelial source of IL-25 in the intestine, where they control ILC2 expansion and downstream IL-13–dependent goblet cell metaplasia (12–14). Brush cells (BrCs) are similar chemosensory EpCs in the trachea and proximal bronchi that respond to airborne irritants by activating a neural reflex and reducing the respiratory rate (15–17). BrCs, like tuft cells, express elements of the bitter taste transduction system, including Gα-gustducin and transient receptor potential melastatin 5 (TRPM5) (17), but a role for BrCs in type 2 airway inflammation has not been reported, and their numbers in the respiratory mucosa are very low at baseline. Furthermore, despite the advances in understanding chemosensory cell effector functions, the receptors that mediate chemosensory cell activation and expansion beyond taste receptors in any compartment remain largely unknown.

Here, we define the transcriptional signature of naïve airway BrCs, which express high levels of IL-25, IL-10, and IL-18 and the enzymatic pathway required for the generation of CysLTs, but express low levels of IL-33 and TSLP. We find that, in response to inhalation of common aeroallergens that elicit CysLT generation and type 2 cytokine induction, airway BrCs expand in a CysLT-dependent fashion. Of the three CysLTRs, $CysLT_3R$ expression is up-regulated in concert with BrC-specific genes and regulates their expansion in response to

inhalation of either $LTE_4$ or aeroallergens. Furthermore, inhalation of $LTE_4$ alone is sufficient to drive BrC expansion in an IL-25–dependent but signal transducer and activator of transcription 6 (STAT6)–independent fashion, identifying an IL-13– independent pathway of airway EpC remodeling. Last, both *Alternaria* and $LTE_4$-elicited $CysLT_3R$-dependent lung inflammation required IL-25, emphasizing the importance of this BrC activation pathway for airway inflammation and remodeling and defining $CysLT_3R$ as an upstream regulator of BrC function.

## RESULTS

### BrCs are unique among airway EpCs and the dominant source of IL-25

We imaged the tracheal epithelium in whole mounts and confirmed that a population of airway EpCs in the trachea express the tuft cell markers doublecortin-like kinase 1 (DCLK1) and Gα-gustducin (Fig. 1A). Airway BrCs are heterogeneous in their expression of classic BrC markers and choline acetyltransferase (ChAT) (15). To confirm that DCLK1 marks the ChAT-expressing airway BrCs, we evaluated tracheas of $ChAT^{BAC}$-eGFP (enhanced green fluorescent protein) mice (18). In these mice, the majority of $DCLK1^+$ cells were ChAT-$eGFP^+$ (91 ± 1%), and most ChAT-$eGFP^+$ cells were $DCLK1^+$ (86 ± 1%), confirming that they are cholinergic chemosensory BrCs (Fig. 1B and fig. S1A). $DCLK1^+$ BrCs were not immunoreactive for the ciliated EpC marker acetylated α-tubulin (ACT), the secretory EpC marker club cell secretory protein (CCSP), or neuroendocrine EpC marker calcitonin generelated peptide (CGRP; fig. S1B). Many BrCs were closely intertwined with $CGRP^+$ nerve fibers (fig. S1B). To evaluate the IL-25–generating capacity of BrCs, we used $Il25^{F25/F25}$ mice that express tandem dimer red fluorescent protein (RFP) from the *Il25* locus (14).

Nearly all $DCLK1^+$ cells were IL-25–$RFP^+$ (99.2 ± 0.2%), whereas 93% of the IL-25–$RFP^+$ cells were $DCLK1^+$ (93 ± 2%; Fig. 1C and fig. S1A). Together, these data suggest that these chemosensory cells are poised to sense airway luminal contents, transmit signals to surrounding nerves, and initiate inflammation through IL-25 release.

To further define their capacity relative to other EpCs and hematopoietic cells resident in naïve tissue, we isolated epithelial cell adhesion molecule $(EpCAM)^+CD45^-eGFP^+$ cells from the trachea of naïve $ChAT^{BAC}$-eGFP mice, along with $EpCAM^+CD45^-eGFP^-$ EpCs and $CD45^+$ cells, and performed low-input RNA sequencing (RNA-seq; fig. S1C). ChAT-$eGFP^+$ BrCs comprised 0.5% of all $EpCAM^+CD45^-$ cells. Less than 1% of ChAT-$eGFP^+$ cells expressed CD45 in contrast to reports of $CD45^+$ expression on intestinal tuft cells (19). $EpCAM^+$ $CD45^-eGFP^-$ (referred to as $EpCAM^+$ for simplicity) cells were composed of a mixture of airway EpCs as evidenced by their expression of the secretory cell gene *Scgb1a1*, the ciliated cell-specific gene *Foxj1*, and the basal cell-specific genes *Krt5* and *Krt14* (fig. S1D). Airway ChAT-eGFP cells were enriched with a false discovery rate (FDR) of <0.05 for 74 of the 94 genes recently identified as a consensus intestinal tuft cell signature (fig. S1E) (19). Of the 20 that were not significantly enriched, no expression was detected for 6 in tracheal BrCs (*Ffar3*, *Mlip*, *Smpx*, *Siglecf*, *Lect2*, and *Agt*). When compared with $EpCAM^+$ EpCs and with $CD45^+$ cells in the airway, principal components analysis demonstrated that BrCs grouped quite distinctly (Fig. 1D). This BrC distinction relative to $EpCAM^+$ cells was

further reflected in the notable total number of highly differentially expressed genes (Fig. 1E). This included 1305 genes expressed at four-fold or higher levels in EpCAM $^{+}$eGFP$^{+}$ cells (BrCs; Fig. 1E, high-lighted in purple), of which 418 genes were expressed at 32-fold or higher levels in BrCs (Fig. 1E, highlighted in red). As expected, a large number of taste receptors, their associated signal transduction system, and the acetylcholine synthesis enzymes *Pld2* and *Chat* were enriched in BrCs (Fig. 1F).

BrCs expressed remarkably high levels of three transcripts encoding critical enzymes of the CysLT biosynthetic pathway including *Alox5* (5-LO), *Alox5ap* (5-LO–activating protein), and *Ltc4s* ($LTC_4S$), as well as *Pla2g4a* (phospholipase A2, group IVA; Fig. 1, F and G), suggesting that BrCs are poised to rapidly generate CysLTs in response to relevant stimuli in the airway. We confirmed that *Il25* is highly enriched in BrCs and found that its receptor *Il17rb* is also differentially expressed in BrCs, even when compared with resident hematopoietic cells, suggesting that an autocrine loop might be operational in BrCs. Although *Tslp* was expressed at low levels in BrCs (fig. S1F), *Il33* and its receptor *Il1rl1* were not detected in BrCs but were expressed as expected in EpCs and hematopoietic cells, respectively (Fig. 1G). BrCs expressed *Il18*, *Il10*, and *Cxcl12* at levels similar to those of airway resident hematopoietic cells (Fig. 1G), indicating that BrCs are poised to control airway immune responses through the production of cytokines and chemokines. These mediators were not detected in a recent report of intestinal tuft cells (19), which might suggest a difference between chemosensory cells in the two compartments or be reflective of different sequencing approaches. Using the RIKEN database for transcriptional regulators (http://genome.gsc.riken.jp/TFdb/), we found high expression of the transcription factors *Pou2f3 and Gfi1b*, previously reported to control one or both chemosensory populations (Fig. 1H) (12, 20–22). We further observed several homeobox family transcription factors (23, 24), implicated in neural development, and high levels of *Spdef*, the master regulator of airway goblet cell development (25).

## Common aeroallergens induce BrC expansion in a CysLT-dependent fashion

To understand whether the airway BrC compartment might be dynamic in response to type 2 stimuli, we challenged mice with the common aeroallergen *Alternaria*, which induces both CysLT generation and STAT6-dependent innate immune cell activation (6, 9, 26). After a single inhalation of *Alternaria*, DCLK1$^{+}$ BrCs expanded in the trachea of wild-type (WT) mice as early as 3 days later and were found in clusters of two to four cells (Fig. 2, A and D). *Alternaria*-elicited BrC expansion was partially impaired in *Stat6* $^{-/-}$ mice (Fig. 2, B and D). We and others have reported an upstream role for CysLTs in driving airway type 2 inflammation (5, 9 ), and thus we next assessed mice with a genetic deletion of $LTC_4S$, the terminal enzyme in CysLT biosynthesis. *Alternaria*-elicited BrC expansion was negligible in *Ltc4s*$^{-/-}$ mice (Fig. 2, C and D), and no clusters of BrCs were detected, indicating CysLT regulation of this compartment. *Ltc4s*$^{-/-}$ mice, unlike *Stat6*$^{-/-}$ mice, had a trend to higher baseline numbers of BrCs that was confirmed in additional experiments (Fig. 2E), suggesting a possible role for CysLTs in regulating BrC homeostasis. A single inhalation of the dust mite allergen *Df* also elicited CysLT-dependent BrC expansion in the trachea by 3 days after challenge (Fig. 2E), indicating that BrC expansion can be elicited by other allergens that induce CysLT generation (27).

## $CysLT_3R$, a tracheal EpC receptor, regulates allergen-induced BrC expansion

Our previous studies in the nose had established that the early epithelial effects of CysLTs are mediated through the high-affinity $LTE_4$ receptor, $CysLT_3R$ (6). To determine the relative contributions of the three CysLT receptors to BrC expansion, we first evaluated the transcript levels of these receptors in mice challenged with phosphate-buffered saline (PBS) or *Alternaria*. Although all three receptors were induced by *Alternaria*, we noted that $CysLT_3R$ was highly significantly correlated to the BrC-specific transcripts *Il25*, *Pou2f3*, and *Gnat3* (Fig. 3A). In situ hybridization (ISH) revealed $CysLT_3R$ expression in the tracheal epithelium of naïve WT mice that was absent in the $CysLT_3R$-deficient *Oxgr1*$^{-/-}$ strain (Fig. 3B). X-gal reactivity, marking *Escherichia coli* β-galactosidase that was inserted in the targeted deletion of *Oxgr1* (6), confirmed expression in solitary tracheal EpCs (Fig. 3C). Immunofluorescence studies demonstrated that X-gal reactivity was detected in some, but not all, DCLK1$^+$ cells from *Oxgr1*$^{-/-}$ mice (Fig. 3D and fig. S2) and was also expressed in unidentified neighboring EpCs (Fig. 3D and fig. S2). To evaluate a role for $CysLT_3R$ in regulating BrC expansion, we treated WT and $CysLT_3R$-deficient (*Oxgr1*$^{-/-}$) mice with either *Alternaria* or *Df*. Similar to the results in *Ltc4s*$^{-/-}$ mice, there was no expansion or clustering of BrCs in *Alternaria*- or *Df*-treated *Oxgr1*$^{-/-}$ mice, demonstrating $CysLT_3R$ regulation of airway BrC expansion (Fig. 3, E to G). $CysLT_3R$-deficient mice had significantly higher baseline numbers of BrCs, as observed in *Ltc4s*$^{-/-}$ mice. Collectively, our data indicate that $CysLT_3R$ regulates aeroallergen-induced BrC expansion.

## $CysLT_3R$ regulates BrC expansion through an IL-25–dependent but STAT6-independent pathway

To address the mechanism by which $CysLT_3R$ mediates BrC expansion, we administered its ligand $LTE_4$ intranasally on four consecutive days and assessed BrC numbers 1 day after the last inhalation. $LTE_4$ was sufficient to induce expansion of tracheal BrCs in WT mice, as demonstrated by increased numbers of DCLK1 $^+$ EpCs (Fig. 4, A and B). Similar to our findings with aeroallergen inhalation, $LTE_4$-elicited BrCs were often found in discrete clusters of two or three cells (Fig. 4A). There was no $LTE_4$-elicited BrC expansion or clustering in $CysLT_3R$-deficient mice (Fig. 4B). Unexpectedly, athough $LTE_4$-elicited BrC expansion was entirely absent in *Oxgr1*$^{-/-}$ mice, it was intact in *Stat6*$^{-/-}$ mice (Fig. 4B), indicating that CysLT3R drives a pathway distinct from IL-13. $LTE_4$ challenges in *Il25*$^{F25/F25}$ demonstrated expansion of IL-25–RFP$^+$ cell numbers (Fig. 4, C and D), suggesting that $LTE_4$-elicited expansion of BrCs augments the capacity of the airway epithelium to generate IL-25. $LTE_4$ challenges of *Il25*$^{F25/F25}$ mice did not change the ratio of DCLK1$^+$ (99.2 ± 0.3% of IL-25–RFP$^+$) and IL-25–RFP$^+$ (93.5 ± 1.5% of DCLK1$^+$) cells. Imaging of the tracheal submucosa in *Il25*$^{F25/F25}$ mice did not reveal additional cellular sources of IL-25 in the setting of $LTE_4$-elicited inflammation. Accordingly, administration of an IL-25 blocking antibody concomitantly with $LTE_4$ challenges completely inhibited tracheal BrC expansion in WT mice with no further reduction in *Oxgr1*$^{-/-}$ mice (Fig. 4E). Together, these results suggest that $LTE_4$/$CysLT_3R$ signaling drives BrC expansion through an IL-25–dependent pathway.

### CysLT$_3$R regulates IL-25–dependent type 2 lung inflammation

To understand the possible sequelae of CysLT$_3$R-mediated BrC activation in the lung, we looked for type 2 lung inflammation elicited by LTE$_4$. Repeated inhalation of LTE$_4$ increased lung CD45$^+$ cells in WT mice (Fig. 5A) and was associated with eosinophilia, and CD4 T cell recruitment with each of these parameters was reduced in CysLT$_3$R-deficient mice. Lung lin$^-$CD45$^+$Thy1.2$^+$ICOS$^+$CD44$^+$ ILC2s (Fig. 5A) and macrophages (CD45$^+$SiglecF$^+$CD11c$^+$CD11b$^-$; fig. S3D) were also expanded in WT mice but not in CysLT$_3$R-deficient mice. LTE$_4$- elicited expansion of DCs (CD11c$^+$MHCII$^+$SiglecF$^-$) was CysLT$_3$R-independent, suggesting a selective effect on some populations (fig. S3D). Antibody-mediated blockade of IL-25 reduced LTE$_4$-elicited lung CD45$^+$ cells and lung eosinophils, as compared with isotype control (Fig. 5B). Anti– IL-25 treatment also reduced LTE$_4$-elicited IL-25–dependent killer cell lectin-like receptor subfamily G member 1 (KLRG1$^+$) ILC2s (28), demonstrating the importance of the IL-25/BrC program for LTE$_4$-driven ILC2 expansion. IL-25 blockade did not reduce the CD4$^+$ T cells or unfractionated ILC2 (lin$^-$CD45$^+$ Thy1.2$^+$ICOS$^+$CD44$^+$) population (fig. S3E), indicating additional pathways for LTE$_4$-elicited ILC2 and CD4 T cell expansion. Whereas LTE$_4$-induced BrC expansion was independent of STAT6 (Fig. 4B), LTE$_4$-elicited inflammation was nearly abolished in *Stat6* $^{-/-}$ mice (fig. S4), highlighting divergent IL-25–dependent pathways for epithelial and hematopoietic effects elicited by LTE$_4$ (fig. S5). *Alternaria*-elicited lung inflammation, eosinophilia, ILC2 cell expansion, and CD4 T cell recruitment were also reduced in CysLT$_3$R-deficient mice (Fig. 5C) and depended on IL-25 (Fig. 5D). There was no further reduction of *Alternaria*-induced inflammation in *Oxgr1*$^{-/-}$ mice treated with IL-25 antibody, suggesting that IL-25 mediates the CysLT$_3$R-dependent inflammation. Antibody blockade of IL-25 reduced but did not abolish *Alternaria*-elicited eosinophilia, which is likely due to the effect of IL-33, a dominant regulator of *Alternaria*-induced ILC2 activation and type 2 inflammation (29, 30). Collectively, these data indicate the relevance of the CysLT$_3$R/BrC/IL-25 pathway to pulmonary inflammation elicited by fungal aeroallergens.

## DISCUSSION

BrCs are sentinel EpCs, classified heretofore as “chemosensory” with the expression of bitter taste receptors and the capacity to activate neural sensory circuits. Here, we identify LTE$_4$ as a previously unrecognized driver of BrC expansion and subsequent IL-25–dependent inflammation, mediated through CysLT$_3$R. These findings indicate that LTE$_4$-activated BrCs have potent immune effector functions, which was unexpected given the rarity of this cell type in the respiratory mucosa. Moreover, we find that this system can be activated by several common aeroallergens that elicit endogenous CysLT generation through distinct pathways in DCs (5), mast cells (6), and possibly BrCs themselves (Fig. 1). Thus, CysLT-dependent BrC activation allows for a conserved EpC response to diverse luminal antigens that extend beyond agonists of the bitter taste receptor system. Because significant levels of CysLTs and IL-25 are generated in response to respiratory viral infection (31–35), our results identify a ligand and receptor pair that may fine-tune BrC reactivity to the broader airway microenvironment.

A remarkable finding in our study is the extent to which BrCs are distinct from other EpCs and from resident immune cells in the airway mucosa, likely reflecting their unique development in association with the neuron sensory system. Our RNA-seq data set demonstrates widespread expression of transcriptional regulators including the Hoxa family, with critical roles in spatiotemporal embryonic patterning and shaping neural synaptic circuits (23, 24). With regard to their immune functions, we would highlight that, in addition to *Il25*, BrCs express high levels of transcripts encoding IL-18, important in eliciting interferon-γ and patterning $T_H1$ immunity (36); C-X-C motif chemokine ligand 12 (CXCL12)/stromal cell–derived factor 1, important in lymphocyte recruitment and activation (37); and IL-10, with immunoregulatory roles (38). Given the broad expression of activating taste receptors on BrCs, future studies that determine the selectivity of generation of these mediators in response to diverse agonists will be of central interest. We did observe mediators (IL-10, IL-18, and CXCL12) and transcriptional regulators (Sox and Hox family transcription factors) that were not identified in intestinal tuft cells (19). Whether this relates to chemosensory cell diversity or the lower sensitivity of single-cell analysis remains to be seen.

We found that murine airway BrCs can expand through a STAT6-independent pathway elicited by $LTE_4$. Whereas the pathways driving BrC expansion in the airways were previously unknown, a well-established STAT6- and ILC2-dependent feed-forward loop is required for the expansion of the chemosensory tuft cell compartment in the intestine. Tuft cell–derived IL-25 induces the activation of ILC2s for generation of IL-13, which, in turn, activates a STAT6-dependent EpC progenitor to differentiate into tuft cells (12–14). Our findings suggest that a similar STAT6-dependent pathway can contribute to BrC expansion triggered by *Alternaria* inhalation, but that it is not required with repeated inhalation of $LTE_4$, likely reflecting a distinct pathway for IL-25 generation and autocrine BrC expansion driven by $LTE_4$ (fig. S5). Although further study is required to determine whether IL-13 and $LTE_4$ act at different stages of BrC development, our findings for $LTE_4$-induced STAT6-independent BrC expansion give a clue as to how EpC remodeling, frequently regarded as a downstream product of type 2 inflammation, can develop independently from canonical IL-13 signaling.

Our study raises several questions that remain unanswered. BrCs can directly activate cholinergic sensory neurons, but whether $LTE_4$ or endogenously generated CysLTs can trigger the neural sensory network and attendant functions that BrCs are so poised to regulate (15, 16, 39) remains to be elucidated. In addition, whereas we find $CysLT_3R$ expression in the upper (6) and lower airways to be restricted to the epithelium, only a subset of BrCs express $CysLT_3R$; interestingly, uncharacterized cells directly adjacent to BrCs are also positive for $CysLT_3R$. Although this may be explained by the significant heterogeneity reported in both BrCs and intestinal tuft populations (16, 40), we do note that BrCs express high levels of the stem cell marker Lgr5, raising the possibility that $CysLT_3R$ might specifically regulate both BrCs and their lineage-negative immediate precursors.

Structural changes in the airways, termed airway remodeling, are a recognized feature of asthma and other chronic inflammatory airway diseases. Although murine tracheal BrCs are a relatively static population in the naïve state (41), here we detected both allergen-and

$LTE_4$-elicited BrC expansion as early as day 3 in the trachea, indicating that some changes in EpC composition can occur quite rapidly. Whether these newly developed $DCLK1^+$ cells have the capacity to produce lipid mediators and cytokines and activate the cholinergic sensory system remains to be elucidated. However, we did find that rapid BrC expansion was linked to the capacity to generate IL-25 and IL-25–dependent lung inflammation. Thus, $CysLT_3R$-driven BrC expansion is an early feature of EpC remodeling that can both shape airway inflammation and confer enhanced recognition of inhaled allergens, pathogens, or commensal organisms.

Last, $LTE_4$ is generated in the setting of viral exacerbations of asthma (42) and in infants with no preceding lung disease (31–34), suggesting that CysLT generation is integral to the innate immune response in human airways. $LTE_4$ alone is sufficient to induce eosinophilia in asthmatics (43) that is independent of $CysLT_1R$ blockade (4). Thus, uncovering a previously unappreciated function for $CysLT_3R$ in directing an EpC program to expand and activate BrCs could have significant pathobiologic and therapeutic implications for a range of human lung diseases.

## MATERIALS AND METHODS

### Study design

The aim of this study was to define the role of $LTE_4$ and its receptor, $CysLT_3R$, in aerollergen-driven BrC expansion and IL-25–dependent type 2 immunity. We characterized the transcriptional profile of murine tracheal BrCs compared with other EpCs using low-input RNA-seq on sorted cells from a fluorescent BrC reporter mouse. To delineate the contribution of $LTE_4$ to BrC expansion and BrC-derived IL-25–dependent type 2 inflammation, we characterized two murine models of aeroallergen-induced innate inflammation (*Df* and *Alternaria*) and a pharmacologic model with $LTE_4$ inhalation in strains lacking the enzyme required for CysLT generation or lacking $CysLT_3R$.

### Experimental model and mice

**Mice—**C57BL/6 *Oxgr1*$^{+/-}$ [Oxgr1$^{tm1(KOMP)Vlcg}$] mice were obtained from the National Institutes of Health Knock-Out Mouse Project (KOMP) and intercrossed to obtain *Oxgr1*$^{-/-}$ mice (11). *Ltc4s*$^{-/-}$ mice were generated on a 129Sv background (44) and backcrossed for 15 generations onto the C57BL/6 background. WT littermates from the intercrossing of *Oxgr1*$^{-/-}$ and *Ltc4s*$^{-/-}$ or age- and sex-matched C57BL/6 mice (Charles River Laboratories, Wilmington, MA) were used as controls. *Stat6*$^{-/-}$ mice [B6.129S2(C)-Stat6<tm1Gru>/J], $ChAT^{BAC}$-eGFP [B6.Cg-Tg(RP23–268L19-EGFP)2Mik/J], and WT C57BL/6J controls were purchased from the Jackson Laboratory (Bar Harbor, ME). *Il25*$^{F25/F25}$ mice were generated as described previously (14). Mice were bred and housed in a specific pathogen-free facility at the Dana-Farber Cancer Institute, Brigham and Women's Hospital, and University of Washington; pups were weaned between 19 and 28 days old. Purchased mice were used for experiments after at least 4 weeks in the same mouse facility. Male and female mice 3 to 8 months of age were used. All mice were housed in groups of four to five mice per cage with a standard 12-hour light, 12-hour dark cycle and provided food and water ad libitum. All experiments were performed during the day. The use of mice for these studies

was in accordance with review and approval by the Animal Care and Use Committee of the Dana-Farber Cancer Institute, Brigham and Women's Hospital, and University of Washington.

### Aeroallergen and LTE4 challenge protocols

Mice received a single intranasal application of 30 μg of *Alternaria alternata* culture filtrate (lot no. 151774) or 100 μg of *Df* extract (lot no. 245566; Greer Laboratories, Lenoir, NC) after anesthesia with an intraperitoneal injection of ketamine (10 mg/kg) and xylazine (20 mg/kg) for full sedation. The aeroallergen extracts were delivered in a total volume of 20 μl of sterile PBS. Mice were euthanized at the indicated time points with isoflurane overdose, and tissues were harvested for histology and fixed with 4% paraformaldehyde (PFA) or digested for flow cytometry. In a separate set of experiments, 0.25 nmol of $LTE_4$ (Cayman Chemical, Ann Arbor, MI) was dissolved and diluted in 20 μl of PBS after ethanol was evaporated and immediately administered intranasally. Mice of a given genotype were randomized to treatment dose, and challenges were performed in groups organized by genotype and treatment dose.

For IL-25 blocking experiments, mice were given an intraperitoneal injection of 100 μg of IL-25 blocking antibody (Clone 35B) or immunoglobulin G1k (IgG1k) isotype antibody (both from BioLegend) 6 hours before the first challenge with *Alternaria* or $LTE_4$, respectively, and a repeat intraperitoneal injection of the antibody or isotype control 48 hours later. Mice were euthanized at the indicated time points with isoflurane overdose, and tissues were harvested for histology and fixed with 4% PFA or digested for flow cytometry.

### In situ hybridization

Paraffin sections (6 μm) were prepared from perfused mouse trachea and lung, and ISH was performed using the ViewRNA ISH Tissue 1-Plex Assay Kit (Affymetrix) following the manufacturer's protocol. Briefly, samples were heated in pretreatment solution for 10 min (lung) or 20 min (trachea), followed by protease digestion for 10 min. Sections were hybridized with mouse Oxgr1 viewRNA Tissue Probe set (VB1–11300-VT, Affymetrix) for 3 hours at 40°C. After hybridization, samples were rinsed with wash buffer (Affymetrix) and amplified through two sequential hybridization steps with an amplifier diluent for 15 to 25 min each. Sections were then incubated with alkaline phosphatase–conjugated oligonucleotide in aqueous buffered solution for 15 min, and positive hybridization was detected with Fast Red substrate. Each step was followed by a rinse in wash buffer (Affymetrix kit), and counterstain was performed with Gill's hematoxylin. Visualization was performed with a Leica DM LB2 microscope equipped with a Nikon DXM 1200 camera.

### Confocal microscopy of whole tracheal mounts and quantitative assessment of BrCs

After fixation with 4% PFA, tracheas were permeabilized in a PBS-based blocking buffer containing 0.1% Triton X-100, 0.1% saponin, 3% bovine serum albumin, and 3% normal donkey serum for 3 hours (13). Primary rabbit anti-DCLK1 antibody (Abcam) was added directly to the blocking buffer for incubation at 4°C for 48 to 72 hours. Tracheas were rinsed with PBS containing 0.1% Triton X-100 for 3 to 4 hours, immunoreactivity to DCLK1 was detected with secondary donkey anti-rabbit antibody conjugated to Alexa Fluor 594 (Life

Technologies) after incubation for 72 hours at 4°C. Nuclear staining was performed with Hoechst 33342 nuclear stain (Sigma-Aldrich). For double-labeling experiments with CCSP, ACT, anti-GFP, and anti-CGRP antibody, the samples were incubated with both primary anti-bodies, followed by the appropriate secondary antibodies labeled with Alexa Fluor 488 or Alexa Fluor 594. For double-labeling experiments with rabbit anti–Gα-gustducin, residual rabbit immunoreactivity in DCLK1-stained tracheas was blocked for 48 hours with unlabeled donkey anti-rabbit Fab (Jackson ImmunoResearch) diluted 1:50 in blocking solution, followed by rabbit anti–Gα-gustducin and immunodetection with a donkey anti-rabbit (Life Technologies) for 48 to 72 hours each. For double-labeling experiments with rabbit anti-RFP in *Il25*$^{F25/F25}$ mice, tracheas were incubated with anti-dsRed antibody (Clontech) and visualized with Alexa Fluor 594 donkey anti-rabbit antibody (Life Technologies). After staining for IL-25–RFP, tracheas were rinsed overnight and residual rabbit immunoreactivity was blocked for 24 hours with rabbit serum (Thermo Invitrogen). DCLK1 immunoreactivity was detected with an Alexa Fluor 488–conjugated antibody to DCLK1 (ab 31704, provided by J. von Moltke). Tracheas were longitudinally split into two halves and embedded with the epithelial surface facing upward using a glycerol-based cover slipping solution. Images were acquired with a Zeiss LSM 700 Laser Scanning Confocal microscope with a 20× Zeiss oil, 0.8 numerical aperture (NA) objective and a 63× Zeiss oil, 1.4 NA objective. The number of BrCs for each animal was enumerated from 6 to 12 photographs corresponding to 1 to 2 $mm^2$ taken from the same areas of each trachea starting at the distal end in proximity to the carina. The total number of DCLK1 immunoreactive cells (ranging from 200 to 600 BrCs in unchallenged mice to 600 to 1200 BrCs in challenged mice) was divided by the area captured in the focal plane to define the number of $DCLK1^+$ cells per square millimeter (table S2). DCLK1 immunoreactive cells and focal plane area were evaluated using ImageJ (National Institutes of Health, Bethesda, MD). Separate images were collected for each fluorochrome and overlaid to obtain a multicolor image.

## BrC isolation and sorting

For single-cell preparations, tracheas were harvested and connective tissue was removed. Tracheas were opened longitudinally and incubated in prewarmed PBS solution containing dispase (16 U/ml; Gibco) and deoxyribonuclease I (DNase I; 20 μg/ml; Sigma-Aldrich) for 30 to 40 min at room temperature with gentle shaking. The first step of digestion was stopped by adding cold Dulbecco's modified Eagle's medium + 5% fetal calf serum (FCS). The tracheas were removed from the solution, and the tracheal epithelium was peeled off with a scalpel under a dissecting microscope. The epithelium was incubated with the remaining submucosa and adventitia in Hepes-Tyrode's buffer without calcium (Boston BioProducts, Boston, MA) containing 20 μl of papain (28 U/mg; Sigma-Aldrich) per milliliter of buffer and 10 μl L-cysteine (25 mg/ml; Sigma-Aldrich) per milliliter of buffer for 30 min at 37°C with gentle agitation. Papain digestion was terminated with Tyrode's solution (Boston BioProducts) with 2 μl leupeptin (5 mg/ml; Sigma-Aldrich) per milliliter of buffer. The digested tissue was vortexed for 30 s and thoroughly triturated using a 21-gauge needle.

Digested cells were passed through a 100-μm filter and washed once before staining for sorting. BrCs identified as $CD45^{-}EpCAM^{+}eGFP^{+}$ cells, $EpCAM^{+}$ EpCs identified as $CD45^{-}EpCAM^{+}eGFP^{-}$ cells, and $CD45^{+}$ cells were separately sorted using monoclonal antibodies (mAbs) against CD45 and EpCAM, after dead cell exclusion with propidium iodide. Cells were sorted at the Brigham and Women's Human Immunology Flow Core using a BD FACSAria Fusion cell sorter. At least 300 but no more than 500 cells from one to two naïve or PBS-treated mouse tracheas were sorted into TCL buffer (Qiagen) supplemented with RNAprotect Cell Reagent (Qiagen).

## Low-input RNA-seq

Cells from tracheal single-cell suspensions were processed at the Broad Institute Technology Labs using low-input eukaryotic Smart-seq2. Briefly, Smart-seq2 libraries were sequenced on an Illumina NextSeq500 using a High Output kit to generate 2 × 25 bp reads (plus dual index reads). Each sample's sequences were aligned using STAR v2.4.2a (45) and the following parameters: --twopassMode Basic, --alignIntronMax 1000000, --alignMatesGapMax 1000000, --sjdbScore 2, --quantMode TranscriptomeSAM, and –sjdbOverhang 24. Alignments were processed using Picard v1.1073 tools to add read groups and other sequencing information, reorder the BAM file to the reference, and mark duplicate sequences. Transcripts per kilobase million (TPM) was then quantified using RSEM v1.2.21 (46) with the paired-end option. The data were assessed for quality using RNA-SeQC (47)

## RNA-seq data analysis

Differential expression analysis of RNA-seq results was conducted using R Bioconductor. Raw counts were derived using the featureCounts function of Rsubread (48). Count normalization and differential expression analysis were conducted using the DESeq2 package (49). Genes were considered to be significantly differentially regulated on the basis of a fold change in expression of >4-fold and an FDR of <0.05 based on a Benjamini-Hochberg adjusted *P* value to correct for multiple comparisons. Principal components analysis was conducted using the top 500 differentially regulated genes by FDR.

## X-gal staining

X-gal staining was performed on mouse tracheas as previously described (6). Visualization was performed in 8-mm deparaffinized sections with a Leica DM LB2 microscope equipped with a Nikon DXM 1200 camera. For colocalization studies, direct visualization of X-gal–stained tissue was achieved after excitation at 633 nm and recording fluorescence emission in the 650 to 770 nm range on an LSM 700 microscope.

## Flow cytometry

Lungs were perfused with 10 ml of cold Hanks' balanced salt solution (HBSS), and the right lower lobe was removed, physically dissociated with a gentleMACS Dissociator (Miltenyi Biotec, San Diego, CA) in 10 ml of RPMI 1640 containing 5% FCS, and then enzymatically dissociated with collagenase (500 U/ml; CLS-IV, Worthington Biochemical), dispase, and DNase I (0.02 mg/ml; Sigma-Aldrich) in RPMI 1640 with 5% FCS at 37°C for 30 min with agitation at 200 rpm. Single cells were harvested by adding another 10 ml of RPMI 1640

with 10% FCS and then collected by centrifugation. Cell suspensions were washed with HBSS and prepared for analysis by flow cytometry. Nonspecific mAb uptake was blocked with CD16/32 (2.4G2; BD Biosciences) for at least 30 min, and appropriate mAb was added for 30 min, followed by Hoechst 33342 for dead cell exclusion. Eosinophils were identified as CD45/CD11b/SiglecF$^+$ cells with high side scatter that were negative for CD11c and major histocompatibility complex II (MHC II; fig. S3A). DCs were identified as SiglecF$^-$CD11c$^+$MHCII$^+$ cells, and macrophages were identified as SiglecF$^+$CD11c$^+$MHCII$^+$CD11b$^-$ cells (fig. S3A). CD4 T cells were identified as T cell receptor β (TCRβ$^+$)CD4$^+$ (fig. S3B). To identify Thy1.2$^+$CD44$^+$ICOS$^+$IL7R$^+$ILC2s, lineage-positive cells were excluded using mAb against CD19, CD8, GR1, Fcer1, NK1.1, CD11c, CD11b, TCRβ, and CD4 after identification of CD45$^+$ cells. ILC2 cells were identified as IL7R$^+$Thy1.2$^+$ICOS$^+$CD44$^+$ cells with low forward and side scatter (fig. S3B). KLRG1$^+$ ILCs were separately evaluated using a broader panel of lineage markers including CD19, CD8, GR1, Fcer1, NK1.1, CD11c, CD11b, TCRβ, CD4, TCRγδ, TER119, and CD5 and defined as lineage-negative IL7R$^+$KLRG1$^+$Thy1.2$^+$ cells with low forward and side scatter (fig. S3C).

### Reverse transcription polymerase chain reaction

Whole tracheas and lungs were harvested after mice were bled through the abdominal aorta. Total RNA was isolated with TRIzol Reagent (Invitrogen, Carlsbad, CA) according to the manufacturer's protocol and further purified with the RNeasy Micro Kit (Qiagen). Total RNA (1 μg) was reverse-transcribed with SuperScript III (In-vitrogen), and quantitative reverse transcription polymerase chain reaction (PCR) was performed with primers specific for mouse *Oxgr1*, *Cysltr1*, *Gnat3*, *Il25*, *Pou2f3*, or 18S ribosomal RNA (rRNA; Qiagen) or *Cysltr2* (Sigma-Aldrich) using Brilliant II SYBR Green QPCR Master Mix with Low ROX and amplification with the Mx3005P Real-Time PCR System (Agilent Technologies, Santa Clara, CA) under the following conditions: 98°C for 15 s, 60°C for 30 s, 40 cycles. The ratio of each mRNA relative to the 18S rRNA was calculated with the $\Delta\Delta C_t$ method.

### Statistics

Analysis was performed with GraphPad Prism software (version 5.01, GraphPad, La Jolla, CA). Nonparametric two-sided Mann-Whitney tests were used to determine significance in pairwise comparison of responses in the in vivo models. Data indicate means ± SEMs in all bar graphs. Correlations were performed using linear regression and Spearman correlation. For RNA-seq analysis, hypergeometric distribution was calculated using the R stats package. $P < 0.05$ was considered significant. Sample sizes were not predetermined by statistical methods.

## Supplementary Material

Refer to Web version on PubMed Central for supplementary material.

## Acknowledgments:

We thank R. Locksley (University of California, San Francisco) for providing *Il25*$^{F25/F25}$ mice and A. Hill (Boston Children's Hospital Intellectual and Developmental Disabilities Research Center Cellular Imaging Core), T. Bowman, C. Unitt, and N. Kedersha for help with trachea whole-mount imaging. The *Il25*$^{F25/F25}$ mice are available from R. Locksley under a material transfer agreement with University of California, San Francisco. The

*Oxgr1*$^{-/-}$ mice are available from the NIH Knock-Out Mouse Program under a material transfer agreement with University of California Davis.

**Funding:** This work was supported by NIH grants R01 HL120952 (to N.A.B.), R56 AI 134989 (to N.A.B.), U19 AI095219 (to N.A.B., Y.K., and L.G.B.), K08 AI132723 (to L.G.B.), DP2 OD024087 (to J.v.M.), and T32 AI106677 (J.W.M.). This work was also supported by the American Academy of Allergy, Asthma and Immunology (AAAAI)/American Lung Association (ALA) Respiratory Disease Award (to N.A.B.), by the AAAAI Foundation Faculty Development Award (to L.G.B.), by the Steven and Judy Kaye Young Innovators Award (to N.A.B.), by the Department of Defense Investigator-Initiated Research Award W81XWH-17–1-0527 (to Y.K.), by the Joycelyn C. Austen Fund for Career Development of Women Physician Scientists (to L.G.B.), and by a donation by the Vinik family (to L.G.B.).

## REFERENCES AND NOTES

1. Austen KF, Maekawa A, Kanaoka Y, Boyce JA, The leukotriene E4 puzzle: Finding the missing pieces and revealing the pathobiologic implications. J. Allergy Clin. Immunol 124, 406–414 (2009). [PubMed: 19647860]
2. Manning PJ, Watson RM, Margolskee DJ, Williams VC, Schwartz JI, O'Byrne PM, Inhibition of exercise-induced bronchoconstriction by MK-571, a potent leukotriene D4-receptor antagonist. N. Engl. J. Med 323, 1736–1739 (1990). [PubMed: 2174121]
3. Leff JA, Busse WW, Pearlman D, Bronsky EA, Kemp J, Hendeles L, Dockhorn R, Kundu J. Zhang, Seidenberg BC, Reiss TF, Montelukast, a leukotriene-receptor antagonist, for the treatment of mild asthma and exercise-induced bronchoconstriction. N. Engl. J. Med 339, 147–152 (1998). [PubMed: 9664090]
4. Lazarinis N, Bood J, Gomez C, Kolmert J, Lantz AS, Gyllfors P, Davis A, Wheelock CE, Dahlén SE, Dahlén B, Leukotriene E4 induces airflow obstruction and mast cell activation via the CysLT1 receptor. J. Allergy Clin. Immunol 2018, S0091–6749 (2018).
5. Barrett NA, Rahman OM, Fernandez JM, Parsons MW, Xing W, Austen KF, Kanaoka Y, Dectin-2 mediates Th2 immunity through the generation of cysteinyl leukotrienes. J. Exp. Med 208, 593–604 (2011). [PubMed: 21357742]
6. Bankova LG, Lai J, Yoshimoto E, Boyce JA, Austen KF, Kanaoka Y, Barrett NA, Leukotriene $E_4$ elicits respiratory epithelial cell mucin release through the G-protein– coupled receptor, GPR99. Proc. Natl. Acad. Sci. U.S.A 113, 6242–6247 (2016). [PubMed: 27185938]
7. von Moltke J, O'Leary CE, Barrett NA, Kanaoka Y, Austen KF, Locksley RM, Leukotrienes provide an NFAT-dependent signal that synergizes with IL-33 to activate ILC2s. J. Exp. Med 214, 27–37 (2017). [PubMed: 28011865]
8. Clarke DL, Davis NHE, Campion CL, Foster ML, Heasman SC, Lewis AR, Anderson IK, Corkill DJ, Sleeman MA, May RD, Robinson MJ, Dectin-2 sensing of house dust mite is critical for the initiation of airway inflammation. Mucosal Immunol 7, 558–567 (2014). [PubMed: 24129160]
9. Doherty TA, Khorram N, Lund S, Mehta AK, Croft M, Broide DH, Lung type 2 innate lymphoid cells express cysteinyl leukotriene receptor 1, which regulates $T_H2$ cytokine production. J. Allergy Clin. Immunol 132, 205–213 (2013). [PubMed: 23688412]
10. Lund SJ, Portillo A, Cavagnero K, Baum RE, Naji LH, Badrani JH, Mehta A, Croft M, Broide DH, Doherty TA, Leukotriene C4 potentiates IL-33-induced group 2 innate lymphoid cell activation and lung inflammation. J. Immunol 199, 1096–1104 (2017). [PubMed: 28667163]
11. Kanaoka Y, Maekawa A, Austen KF, Identification of GPR99 protein as a potential third cysteinyl leukotriene receptor with a preference for leukotriene E4 ligand. J. Biol. Chem 288, 10967–10972 (2013). [PubMed: 23504326]
12. Gerbe F, Sidot E, Smyth DJ, Ohmoto M, Matsumoto I, Dardalhon V, Cesses P, Garnier L, Pouzolles M, Brulin B, Bruschi M, Harcus Y, Zimmermann VS, Taylor N, Maizels RM, Jay P, Intestinal epithelial tuft cells initiate type 2 mucosal immunity to helminth parasites. Nature 529, 226–230 (2016). [PubMed: 26762460]
13. Howitt MR, Lavoie S, Michaud M, Blum AM, Tran SV, Weinstock JV, Gallini CA, Redding K, Margolskee RF, Osborne LC, Artis D, Garrett WS, Tuft cells, taste-chemosensory cells, orchestrate parasite type 2 immunity in the gut. Science 351, 1329–1333 (2016). [PubMed: 26847546]

14. von Moltke J, Ji M, Liang H-E, Locksley RM, Tuft-cell-derived IL-25 regulates an intestinal ILC2-epithelial response circuit. Nature 529, 221–225 (2016). [PubMed: 26675736]
15. Krasteva G, Canning BJ, Hartmann P, Veres TZ, Papadakis T, Mühlfeld C, Schliecker K, Tallini YN, Braun A, Hackstein H, Baal N, Weihe E, Schütz B, Kotlikoff M, Ibanez-Tallon I, Kummer W, Cholinergic chemosensory cells in the trachea regulate breathing. Proc. Natl. Acad. Sci. U.S.A 108, 9478–9483 (2011). [PubMed: 21606356]
16. Krasteva G, Canning BJ, Papadakis T, Kummer W, Cholinergic brush cells in the trachea mediate respiratory responses to quorum sensing molecules. Life Sci 91, 992–996 (2012). [PubMed: 22749863]
17. Tizzano M, Cristofoletti M, Sbarbati A, Finger TE, Expression of taste receptors in solitary chemosensory cells of rodent airways. BMC Pulm. Med 11, 3 (2011). [PubMed: 21232137]
18. Tallini YN, Shui B, Greene KS, Deng K-Y, Doran R, Fisher PJ, Zipfel W, Kotlikoff MI, BAC transgenic mice express enhanced green fluorescent protein in central and peripheral cholinergic neurons. Physiol. Genomics 27, 391–397 (2006). [PubMed: 16940431]
19. Haber AL, Biton M, Rogel N, Herbst RH, Shekhar K, Smillie C, Burgin G, Delorey TM, Howitt R, Katz Y, Tirosh I, Beyaz S, Dionne D, Zhang M, Raychowdhury R, Garrett WS, Rozenblatt-Rosen O, Shi HN, Yilmaz O, Xavier RJ, Regev A, A single-cell survey of the small intestinal epithelium. Nature 551, 333–339 (2017). [PubMed: 29144463]
20. Ohmoto M, Yamaguchi T, Yamashita J, Bachmanov AA, Hirota J, Matsumoto I, Pou2f3/Skn-1a is necessary for the generation or differentiation of solitary chemosensory cells in the anterior nasal cavity. Biosci. Biotechnol. Biochem 77, 2154–2156 (2013). [PubMed: 24096675]
21. Yamashita J, Ohmoto M, Yamaguchi T, Matsumoto I, Hirota J, Skn-1a/Pou2f3 functions as a master regulator to generate Trpm5-expressing chemosensory cells in mice. PLOS ONE 12, e0189340 (2017). [PubMed: 29216297]
22. Bjerknes M, Khandanpour C, Möröy T, Fujiyama T, Hoshino M, Klisch TJ, Ding Q, Gan L, Wang J, Martin MG, Cheng H, Origin of the brush cell lineage in the mouse intestinal epithelium. Dev. Biol 362, 194–218 (2012). [PubMed: 22185794]
23. Philippidou P, Dasen JS, *Hox* genes: Choreographers in neural development, architects of circuit organization. Neuron 80, 12–34 (2013). [PubMed: 24094100]
24. Philippidou P, Dasen JS, Sensory-motor circuits: *Hox* genes get in touch. Neuron 88, 437–440 (2015). [PubMed: 26539884]
25. Rajavelu P, Chen G, Xu Y, Kitzmiller JA, Korfhagen TR, Whitsett JA, Airway epithelial SPDEF integrates goblet cell differentiation and pulmonary Th2 inflammation. J. Clin. Invest 125, 2021–2031 (2015). [PubMed: 25866971]
26. Doherty TA, Khorram N, Chang JE, Kim H-K, Rosenthal P, Croft M, Broide DH, STAT6 regulates natural helper cell proliferation during lung inflammation initiated by *Alternaria*. Am. J. Physiol. Lung Cell. Mol. Physiol 303, L577–L588 (2012). [PubMed: 22865552]
27. Barrett NA, Maekawa A, Rahman OM, Austen KF, Kanaoka Y, Dectin-2 recognition of house dust mite triggers cysteinyl leukotriene generation by dendritic cells. J. Immunol 182, 1119–1128 (2009). [PubMed: 19124755]
28. Huang Y, Guo L, Qiu J, Chen X, Hu-Li J, Siebenlist U, Williamson PR, Urban JF Jr., Paul WE, IL-25-responsive, lineage-negative KLRG1$^{hi}$ cells are multipotential 'inflammatory' type 2 innate lymphoid cells. Nat. Immunol 16, 161–169 (2015). [PubMed: 25531830]
29. Kouzaki H, Iijima K, Kobayashi T, O'Grady SM, Kita H, The danger signal, extracellular ATP, is a sensor for an airborne allergen and triggers IL-33 release and innate Th2-type responses. J. Immunol 186, 4375–4387 (2011). [PubMed: 21357533]
30. Bartemes KR, Iijima K, Kobayashi T, Kephart GM, McKenzie AN, Kita H, IL-33-responsive lineage$^{-}$CD25$^{+}$CD44$^{hi}$ lymphoid cells mediate innate type 2 immunity and allergic inflammation in the lungs. J. Immunol 188, 1503–1513 (2012). [PubMed: 22198948]
31. Da Dalt L, Callegaro S, Carraro S, Andreola B, Corradi M, Baraldi E, Nasal lavage leukotrienes in infants with RSV bronchiolitis. Pediatr. Allergy Immunol 18, 100–104 (2007). [PubMed: 17338781]

32. Sznajer Y, Westcott JY, Wenzel SE, Mazer B, Tucci M, Toledano BJ, Airway eicosanoids in acute severe respiratory syncytial virus bronchiolitis. J. Pediatr 145, 115–118 (2004). [PubMed: 15238918]
33. Piedimonte G, Renzetti G, Auais A, Di Marco A, Tripodi S, Colistro F, Villani A, Di Ciommo V, Cutrera R, Leukotriene synthesis during respiratory syncytial virus bronchiolitis: Influence of age and atopy. Pediatr. Pulmonol 40, 285–291 (2005). [PubMed: 16106356]
34. van Schaik SM, Tristram DA, Nagpal IS, Hintz KM, Welliver II RC, Welliver RC, Increased production of IFN-gamma and cysteinyl leukotrienes in virus-induced wheezing. J. Allergy Clin. Immunol 103, 630–636 (1999). [PubMed: 10200012]
35. Beale J, Jayaraman A, Jackson DJ, Macintyre JDR, Edwards MR, Walton RP, Zhu J, Ching YM, Shamji B, Edwards M, Westwick J, Cousins DJ, Hwang YY, McKenzie A, Johnston SL, Bartlett NW, Rhinovirus-induced IL-25 in asthma exacerbation drives type 2 immunity and allergic pulmonary inflammation. Sci. Transl. Med 6, 256ra134 (2014).
36. Garlanda C, Dinarello CA, Mantovani A, The interleukin-1 family: Back to the future. Immunity 39, 1003–1018 (2013). [PubMed: 24332029]
37. Murphy PM, Heusinkveld L, Multisystem multitasking by CXCL12 and its receptors CXCR4 and ACKR3. Cytokine 109, 2–10 (2018). [PubMed: 29398278]
38. Moore KW, de Waal Malefyt R, Coffman RL, O'Garra A, Interleukin-10 and the interleukin-10 receptor. Annu. Rev. Immunol 19, 683–765 (2001). [PubMed: 11244051]
39. Saunders CJ, Christensen M, Finger TE, Tizzano M, Cholinergic neurotransmission links solitary chemosensory cells to nasal inflammation. Proc. Natl. Acad. Sci. U.S.A 111, 6075–6080 (2014). [PubMed: 24711432]
40. McKinley ET, Sui Y, Al-Kofahi Y, Millis BA, Tyska MJ, Roland JT, Santamaria-Pang A, Ohland CL, Jobin C, Franklin JL, Lau KS, Gerdes MJ, Coffey RJ, Optimized multiplex immunofluorescence single-cell analysis reveals tuft cell heterogeneity. JCI Insight 2, 93487 (2017). [PubMed: 28570279]
41. Saunders CJ, Reynolds SD, Finger TE, Chemosensory brush cells of the trachea. A stable population in a dynamic epithelium. Am. J. Respir. Cell Mol. Biol 49, 190–196 (2013). [PubMed: 23526223]
42. Drazen JM, O'Brien J, Sparrow D, Weiss ST, Martins MA, Israel E, Fanta CH, Recovery of leukotriene $E_4$ from the urine of patients with airway obstruction. Am. Rev. Respir. Dis 146, 104–108 (1992). [PubMed: 1320817]
43. Gauvreau GM, Parameswaran KN, Watson RM, O'Byrne PM, Inhaled leukotriene E4, but not leukotriene D4, increased airway inflammatory cells in subjects with atopic asthma. Am. J. Respir. Crit. Care Med 164, 1495–1500 (2001). [PubMed: 11704602]
44. Kanaoka Y, Maekawa A, Penrose JF, Austen KF, Lam BK, Attenuated zymosan-induced peritoneal vascular permeability and IgE-dependent passive cutaneous anaphylaxis in mice lacking leukotriene $C_4$ synthase. J. Biol. Chem 276, 22608–22613 (2001). [PubMed: 11319240]
45. Dobin A, Davis CA, Schlesinger F, Drenkow J, Zaleski C, Jha S, Batut P, Chaisson M, Gingeras TR, STAR: Ultrafast universal RNA-seq aligner. Bioinformatics 29, 15–21 (2013). [PubMed: 23104886]
46. Li B, Dewey CN, RSEM: Accurate transcript quantification from RNA-Seq data with or without a reference genome. BMC Bioinformatics 12, 323 (2011). [PubMed: 21816040]
47. DeLuca DS, Levin JZ, Sivachenko A, Fennell T, Nazaire M-D, Williams C, Reich M, Winckler W, Getz G, RNA-SeQC: RNA-seq metrics for quality control and process optimization. Bioinformatics 28, 1530–1532 (2012). [PubMed: 22539670]
48. Liao Y, Smyth GK, Shi W, The Subread aligner: Fast, accurate and scalable read mapping by seed-and-vote. Nucleic Acids Res 41, e108 (2013). [PubMed: 23558742]
49. Love MI, Huber W, Anders S, Moderated estimation of fold change and dispersion for RNA-seq data with DESeq2. Genome Biol 15, 550 (2014). [PubMed: 25516281]

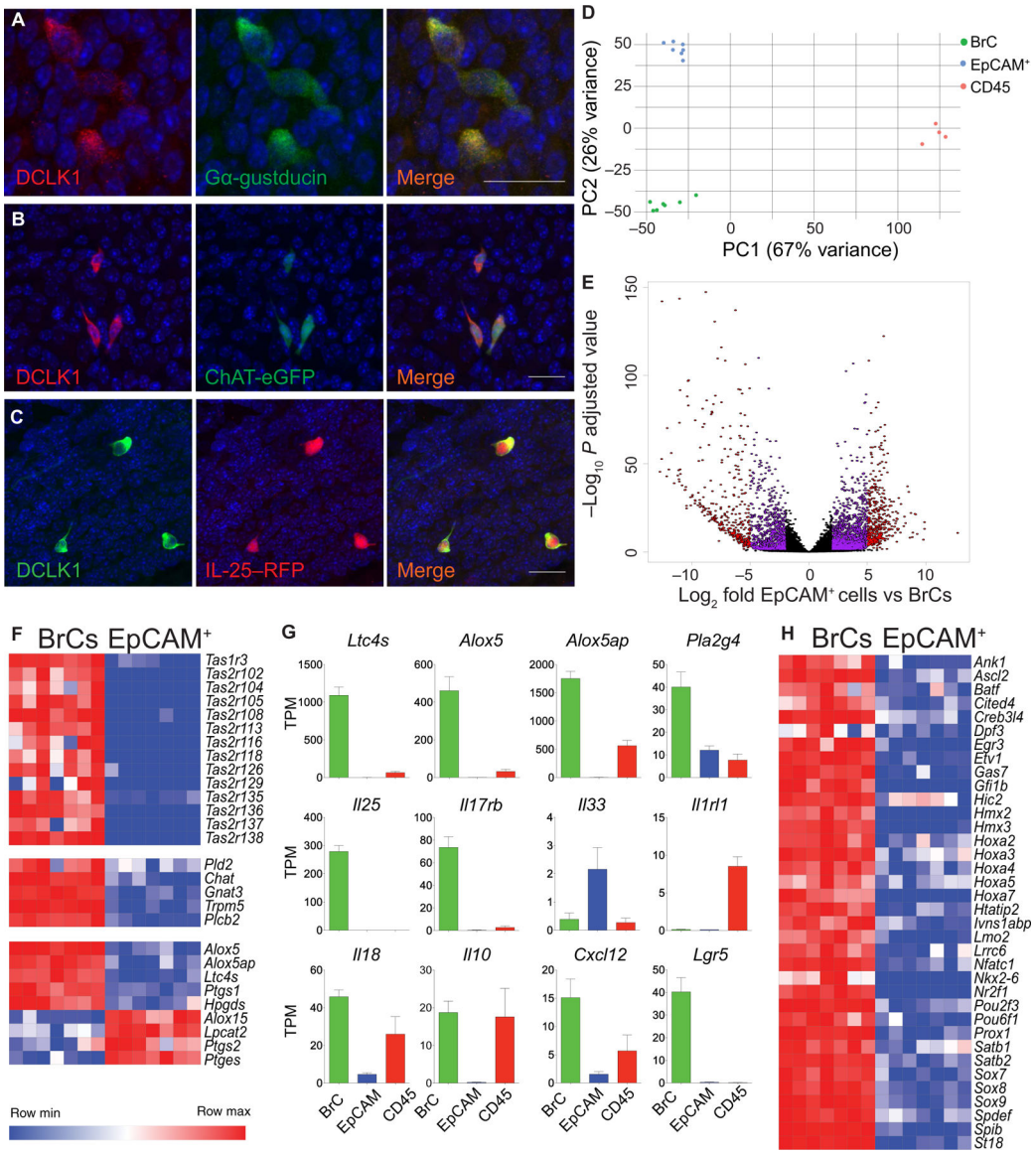


**Fig. 1. BrCs, chemosensory cholinergic cells, express IL-25 and the CysLT generating machinery.**

Tracheas of naïve WT (**A**), ChAT$^{(BAC)}$-eGFP (**B**), and *Il25*$^{F25/F25}$ (**C**) mice were stained for DCLK1, Gα-gustducin, ChAT-eGFP, IL-25–RFP, and Hoechst 33342 (blue). Scale bars, 20 μm. (**D**) Principal components analysis of BrCs (EpCAM$^{+}$CD45$^{-}$eGFP$^{+}$), EpCAM$^{+}$ EpCs (EpCAM$^{+}$CD45$^{-}$eGFP$^{-}$), and resident hematopoietic cells (CD45$^{+}$) analyzed by RNA-seq using the top 500 most variable transcripts. Numbers in parentheses indicate percent variance described by each principal component. (**E** to **H** ) EpCAM$^{+}$ EpC and BrC-enriched transcripts were determined using criteria of fourfold or greater expression in one relative to the other with a *P* adjusted value of <0.05. (E) Volcano plot representing the fold change ($\log_2$ fold change) and FDR ($-\log_{10}$ *P* adjusted value) of differentially expressed genes in EpCAM$^{+}$ EpCs compared with BrCs. Genes highlighted in purple are fourfold differentially expressed. Genes highlighted in red are 32-fold differentially expressed. (F) Transcripts for genes encoding taste receptors, taste receptor signaling machinery, acetyl choline synthesis

machinery, and enzymes involved in lipid mediator generation showing specific enrichment in BrCs compared with EpCAM$^+$ EpCs. (G) Selected genes differentially expressed in BrCs compared with EpCAM$^+$ EpCs and CD45$^+$ cells. *y* axis indicates average of normalized TPM. (H) Transcription factors identified in the RIKEN transcription factor database that are enriched in BrCs compared with EpCAM$^+$ EpCs.

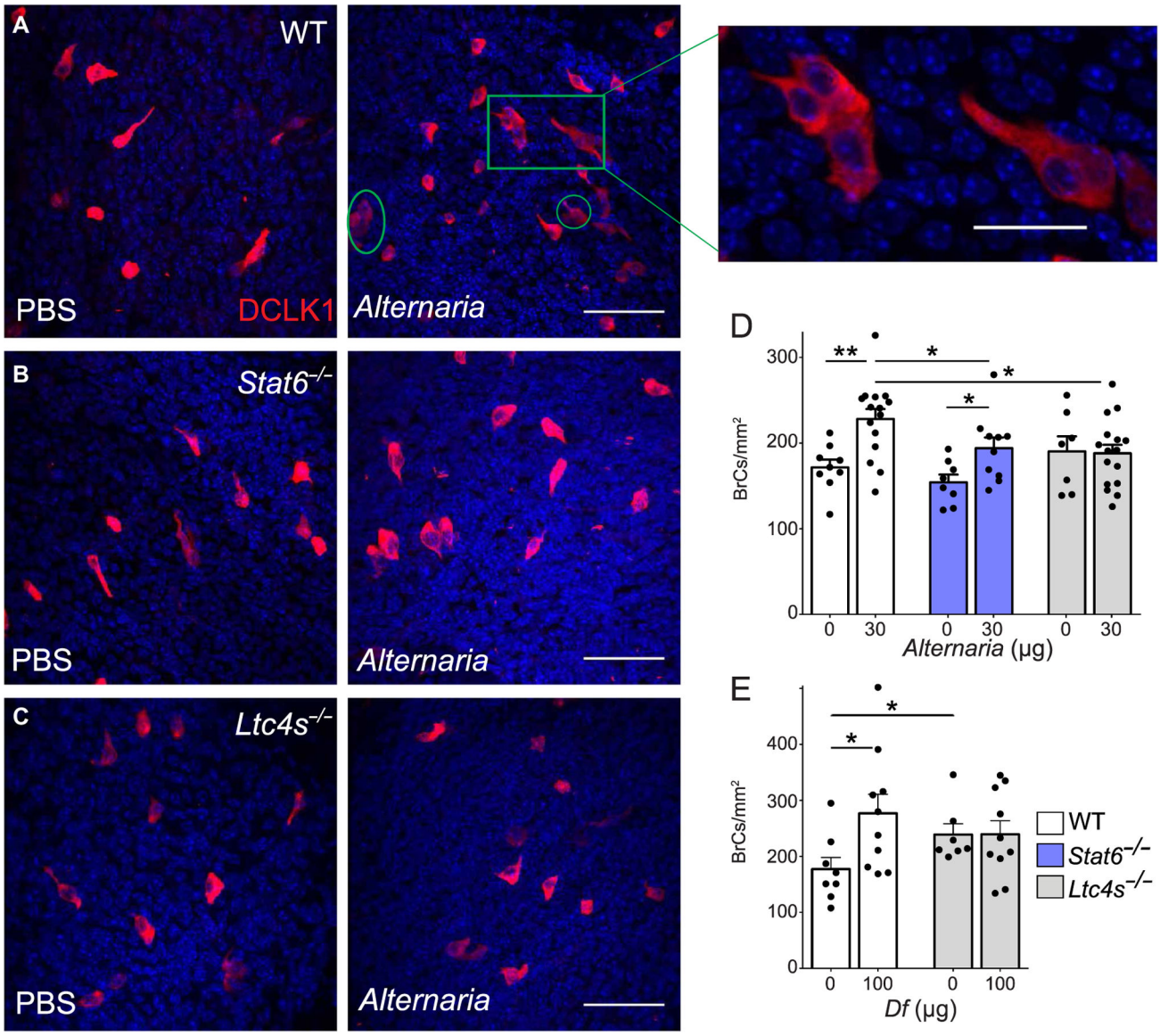


**Fig. 2. Common aeroallergens induce BrC expansion in a CysLT-dependent fashion.**

(**A** to **E**) WT, *Stat6*$^{-/-}$, and *Ltc4s*$^{-/-}$ mice were given a single dose of intranasal *Alternaria*, *Df*, or PBS, and tracheal BrCs were assessed 3 days after the challenge. (A to C) DCLK1 (red) immunofluorescence in the tracheal epithelium from WT, *Stat6*$^{-/-}$, and *Ltc4s*$^{-/-}$ after PBS or *Alternaria* challenges. Circles and the rectangle indicate clusters of DCLK1$^{+}$ cells. Confocal maximum projection images of full-thickness *z*-stacks of the tracheal epithelium in tracheal whole mounts. Scale bar, 50 μm. Right panel represents magnified doublets and triplets from *Alternaria*-challenged WT mice. Scale bars, 20 μm. (D) Immunohistochemical quantitation of BrCs in the trachea of indicated genotypes after challenge with PBS or a 30-μg dose of *Alternaria*. (E) Quantitation of BrCs in the trachea after challenge with a single 100-μg dose of *Df* or PBS. Data in (A) to (C) are representative of at least three experiments, and data in (D) and (E) are means ± SEM from three or more experiments; each circle represents a separate mouse. **P* < 0.05, ***P* < 0.01.

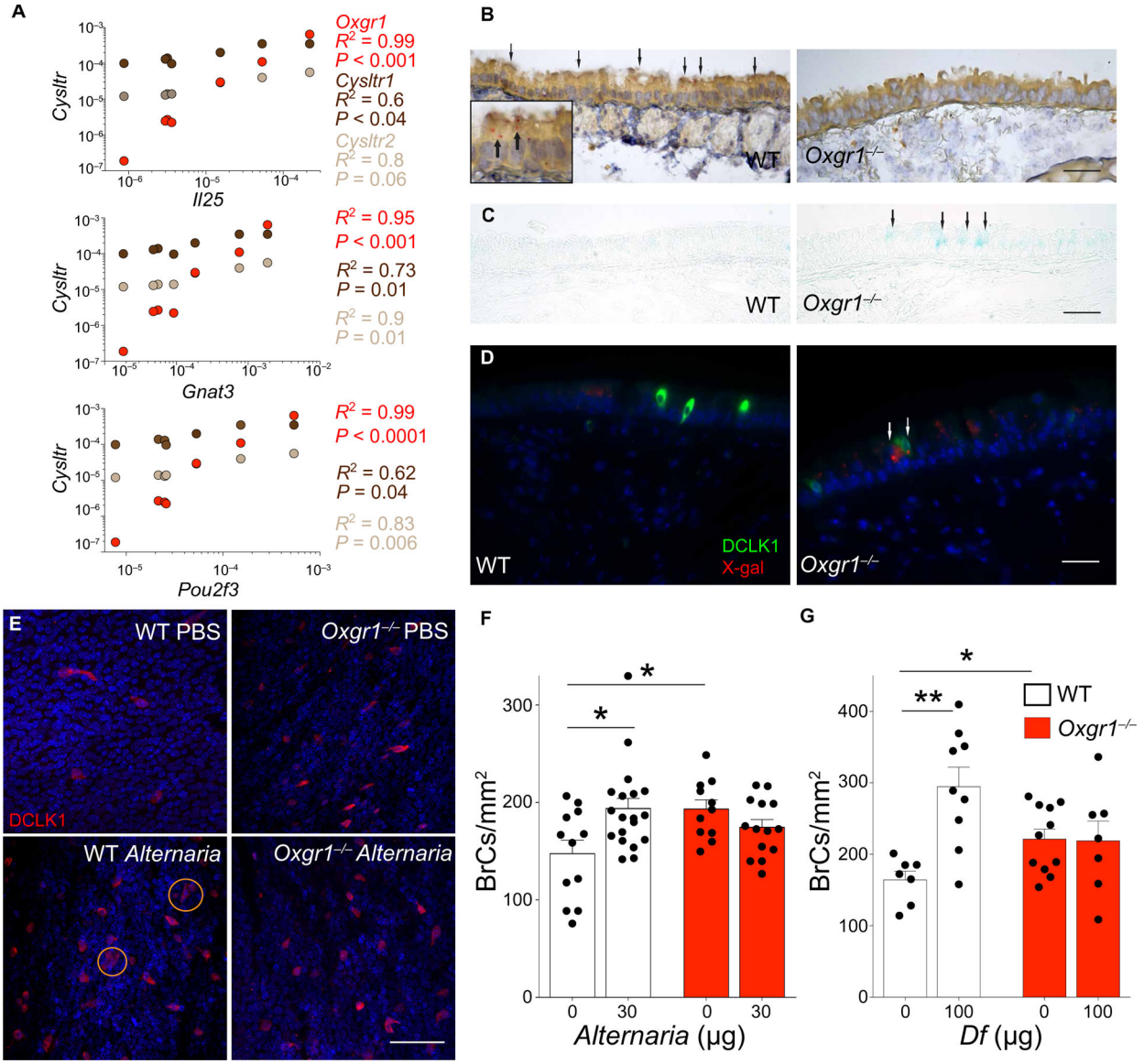


**Fig. 3. CysLT$_3$R is a BrC-associated receptor and regulates aeroallergen-induced BrC expansion.**

(**A** to **G**) WT and *Oxgr1*$^{-/-}$ mice were given a single dose of intranasal *Alternaria*, *Df*, or PBS and were assessed 3 days after the challenge. (A) Transcripts of the three CysLT receptors and indicated BrC-specific genes were assessed in the trachea of PBS- or *Alternaria*-challenged WT mice on day 3 by quantitative PCR. Correlations between CysLTRs and BrC genes were performed using linear regression ($R^2$). (B) ISH for *Oxgr1* in cross sections of trachea from naïve WT and *Oxgr1*$^{-/-}$ mice. Positive red staining in WT mice is indicated by arrows. (C) X-gal reactivity in cross sections of trachea from naïve WT and *Oxgr1*$^{-/-}$ mice. *E. coli* β-galactosidase activity in *Oxgr1*$^{-/-}$ mice produces blue precipitates (arrows) absent in WT mice. (D) Colocalization (arrows) of X-gal reactivity and DCLK1 in cross sections of tracheas from *Oxgr1*$^{-/-}$ mice that carry the targeted insertion of lacZ, encoding *E. coli* β-galactosidase. Scale bars, 25 μm (B to D). (E) DCLK1 immunofluorescence in whole mounts of trachea from WT and *Oxgr1*$^{-/-}$ mice after PBS or

*Alternaria* challenges. Circles indicate clusters of $DCLK1^+$ cells. Confocal maximum projection images of full-thickness *z*-stacks of the tracheal epithelium in tracheal whole mounts. Scale bar, 50 μm. (F and G) Quantitation of BrCs in the trachea of WT and *Oxgr1*$^{-/-}$ mice challenged with *Alternaria* (F) or *Df* (G). Data in (F) and (G) are means ± SEM from at least three experiments; each circle represents a separate mouse. **P* < 0.05, ** *P* < 0.01.

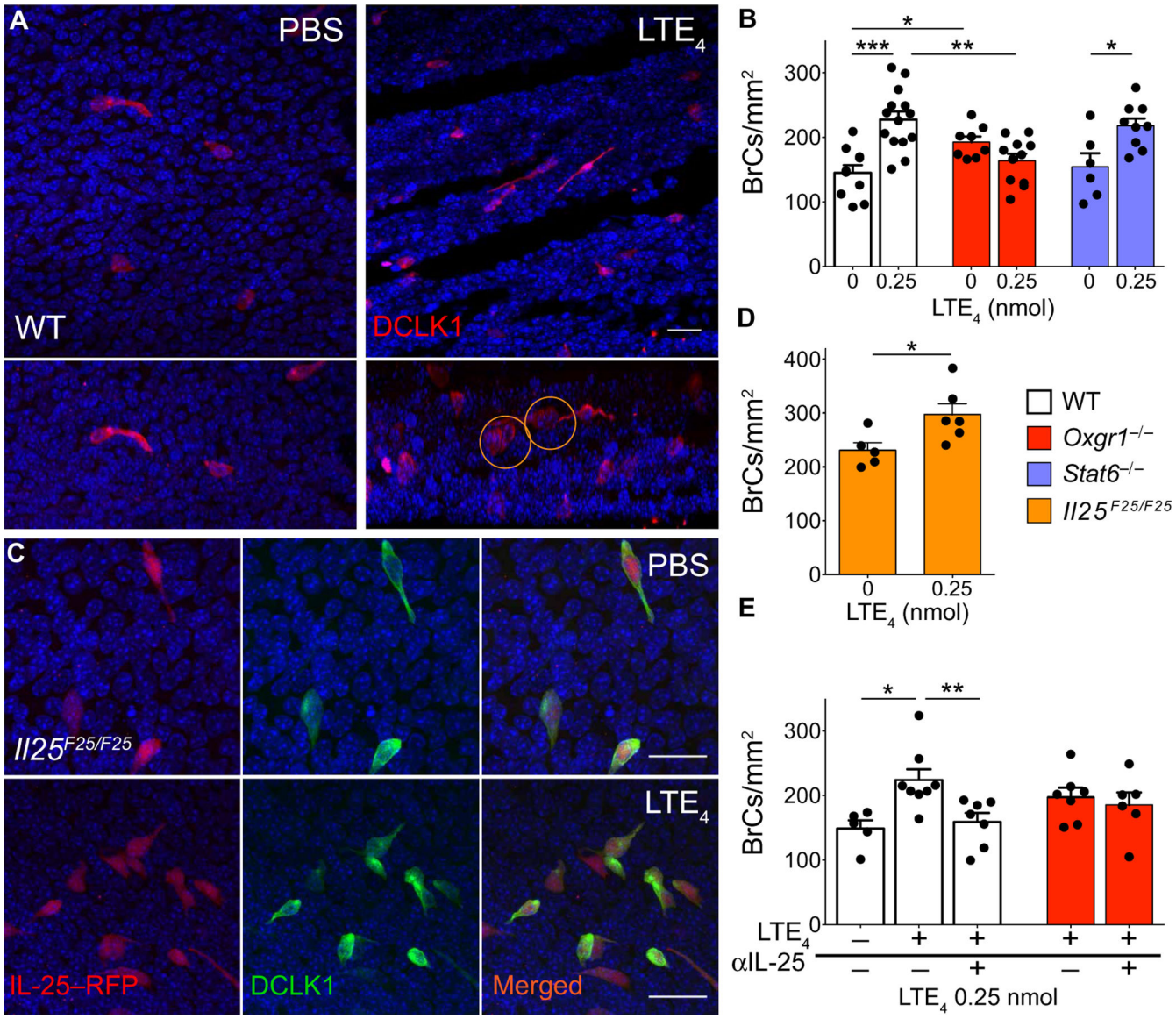


**Fig. 4. CysLT$_3$R regulates BrC expansion through an IL-25–dependent but STAT6-independent pathway.**

(**A** to **E**) WT, *Oxgr1*$^{-/-}$, *Stat6*$^{-/-}$, and *Il25*$^{F25/F25}$ mice were given intranasal LTE$_4$ or PBS daily for 4 days, and DCLK1$^+$ and/or IL-25–RFP$^+$ cells were evaluated in the trachea 24 hours after the last challenge. (A) DCLK1$^+$ cells in the tracheal epithelium of WT mice after PBS or LTE4 challenges; three-dimensional confocal microscopy presenting apical (top) and sagittal (bottom) views of the EpCs derived from full-thickness *z*-stack images of the tracheal epithelium. Circles indicate doublets of DCLK1$^+$ cells. Scale bar, 50 μm. (B) Quantitation of DCLK1$^+$ cells in WT, *Oxgr1*$^{-/-}$, and *Stat6*$^{-/-}$ mice after LTE$_4$ challenges. (C and D) DCLK1$^+$ and IL-25–RFP$^+$ cells in tracheas of *Il25*$^{F25/F25}$ mice with and without challenges with LTE$_4$ and quantitation of cells positive for IL-25–RFP. Scale bars, 25 μm. (E) WT and *Oxgr1*$^{-/-}$ mice were given intranasal LTE$_4$ or PBS challenges as above and injected intraperitoneally with 100 μg of IL-25 antibody (35B) or rat IgG1k on days 0 and 2, and DCLK1$^+$ cells were evaluated in the trachea 24 hours after the last challenge. Results

are means ± SEM pooled from two to three separate experiments. *$P < 0.05$, **$P < 0.01$, ***$P < 0.001$.

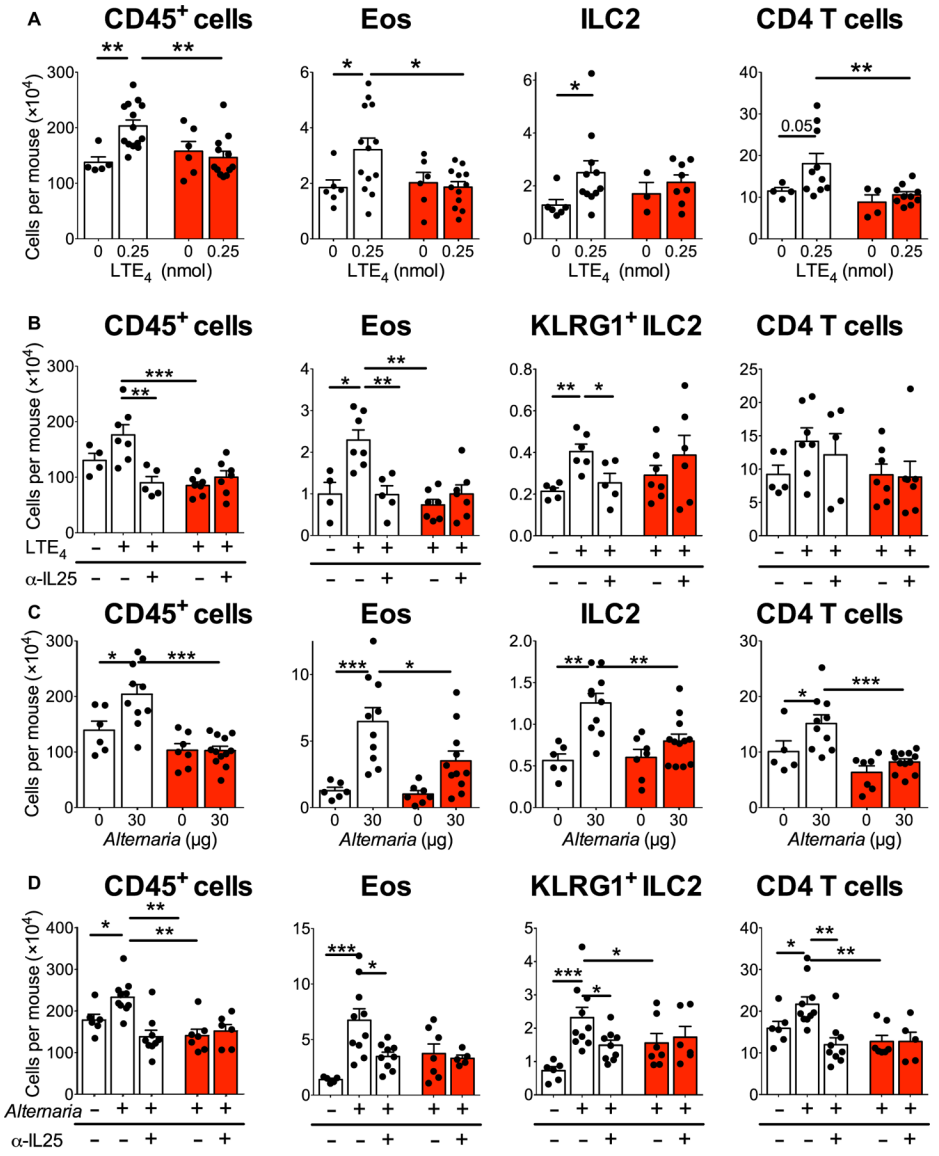


**Fig. 5. CysLT$_3$R regulates IL-25–dependent type 2 lung inflammation.**

(**A**) WT and *Oxgr1*$^{-/-}$ mice were given four daily doses of 0 or 0.25 nmol intranasal $LTE_4$ and analyzed 24 hours after the last inhalation. Flow cytometry analysis of dispersed lung cells showing $CD45^+$ cells, eosinophils ($CD45^+SiglecF^+CD11b^+CD11c^-SSC^{hi}$), ILC2s ($CD45^+lin^-Thy1.2^+CD44^+ICOS^+$), and $CD4^+$ T cells ($CD45^+TCR\beta^+CD4^+$). (**B**) WT and *Oxgr1*$^{-/-}$ mice were given daily $LTE_4$ as above and treated with 100 μg of IL-25 antibody or rat IgG1k on days 0 and 2 intraperitoneally. Lung $CD45^+$ cells, eosinophils, $KLRG1^+$ ILC2s, and $CD4^+$T cells 24 hours after the last $LTE_4$ inhalation. (**C**) WT and *Oxgr1*$^{-/-}$ mice were given a single dose of *Alternaria* (30 μg) or PBS intranasally on day 0. The total number of lung inflammatory cells ($CD45^+$), eosinophils, ILC2s, and CD4T cells was enumerated 3 days later. (**D**) *Alternaria*-treated mice were given IL-25 antibody intraperitoneally on days 0 and 2. The total number of lung inflammatory cells ($CD45^+$), eosinophils, $KLRG1^+$ ILC2s,

and CD4 T cells on day 3. Data are means ± SEM from three experiments; each circle represents a separate mouse. *$P < 0.05$, **$P < 0.01$, ***$P < 0.0001$.